

CD70-Targeted Immuno-PET/CT Imaging of Clear Cell Renal Cell Carcinoma: A Translational Study

Xiang Zhou^{*1}, Qianyun Wu^{*1}, Wei Zhai^{*2}, You Zhang¹, Yanfei Wu³, Min Cao⁴, Cheng Wang¹, Yihui Guan³, Jianjun Liu¹, Fang Xie³, and Weijun Wei¹

¹Department of Nuclear Medicine, Institute of Clinical Nuclear Medicine, Renji Hospital, School of Medicine, Shanghai Jiao Tong University, Shanghai, China; ²Department of Urology, Renji Hospital, School of Medicine, Shanghai Jiao Tong University, Shanghai, China; ³Department of Nuclear Medicine and PET Center, Huashan Hospital, Fudan University, Shanghai, China; and ⁴Department of Thoracic Surgery, Renji Hospital, School of Medicine, Shanghai Jiao Tong University, Shanghai, China

The diagnosis and surveillance of clear cell renal cell carcinoma (ccRCC) remains a clinical challenge. The high and specific expression of the cluster of differentiation 70 (CD70) in ccRCC makes it a potential diagnostic and therapeutic target. **Methods:** We detected and analyzed CD70 expression in various renal cell carcinomas (RCCs) and normal kidneys using immunohistochemical staining. Two novel CD70-specific single-domain antibodies, RCCB3 and RCCB6, were produced and labeled with ⁶⁸Ga to develop radiotracers. We performed immuno-PET/CT imaging with [⁶⁸Ga]Ga-NOTA-RCCB3 and [⁶⁸Ga]Ga-NOTA-RCCB6 in subcutaneous ccRCC patient-derived xenograft models. We recruited 8 RCC patients in a pilot clinical trial (ClinicalTrials.gov identifier: NCT06148220) to evaluate the diagnostic utility of [⁶⁸Ga]Ga-NOTA-RCCB3 and [⁶⁸Ga]Ga-NOTA-RCCB6 immuno-PET/CT. **Results:** Expression of CD70 is associated with sex, tumor differentiation, tumor thrombus, necrosis, distant metastasis, and overall survival of RCC patients. RCCB3 and RCCB6 had high affinities for recombinant human CD70. Immuno-PET/CT imaging with [⁶⁸Ga]Ga-NOTA-RCCB3 and [⁶⁸Ga]Ga-NOTA-RCCB6 rapidly visualized subcutaneous ccRCC with clarity. Tumor uptake of [⁶⁸Ga]Ga-NOTA-RCCB6 was significantly reduced after the blockade of CD70. [⁶⁸Ga]Ga-NOTA-RCCB6 PET/CT in ccRCC patients outperformed traditional ¹⁸F-FDG PET/CT in specifically identifying CD70-positive ccRCC metastases. **Conclusion:** CD70-targeted immuno-PET/CT imaging with [⁶⁸Ga]Ga-NOTA-RCCB6 or [⁶⁸Ga]Ga-NOTA-RCCB3 is a precise and superior method for evaluating tumor burden and suspected metastases in ccRCC patients. This advancement in imaging technology has the potential to improve the clinical decision-making process for this patient cohort significantly.

Key Words: clear cell renal cell carcinoma; CD70; immuno-PET/CT; molecular imaging; single-domain antibody

J Nucl Med 2024; 00:1–8
DOI: 10.2967/jnumed.124.268509

Kidney cancer accounts for around 2.2% of all adult malignancies and is the third most diagnosed urogenital malignancy (1). In adults, more than 90% of kidney cancers are renal cell carcinoma (RCC) (2). Despite advances in diagnosis, 20–30% of patients

already suffer from advanced metastatic disease at the time of diagnosis (3). After receiving radical surgery, 20–30% of patients still develop recurrence or distant metastases (4). Early and precise diagnosis of RCC will improve the management landscape of RCC in terms of early and accurate staging and, more importantly, patient stratification for molecularly targeted therapies and immunotherapies. PET/CT helps diagnose and surveil various cancers. ¹⁸F-FDG is the most commonly used radiotracer in clinical practice (5). However, ¹⁸F-FDG PET/CT has limited value in RCC because of the interference of normally excreted ¹⁸F-FDG and the heterogeneous and low uptake. As a result, ¹⁸F-FDG PET/CT is not routinely recommended for diagnosing RCC (6).

Novel molecular imaging probes for RCC are being developed to target a range of tumor biomarkers, including carbonic anhydrase IX (7). [⁸⁹Zr]Zr-girentuximab, a monoclonal antibody-based radiotracer targeting carbonic anhydrase IX, had demonstrated superior sensitivity and specificity for diagnosing clear cell renal cell carcinoma (ccRCC) in a phase 3 clinical trial (8). However, its clinical application is hindered by the high cost of production, week-long imaging, and potential radiation concerns (9). Molecular imaging tracers with short circulation time for convenient same-day imaging are in high demand. A single-domain antibody (sdAb), the variable domain of a heavy chain-only antibody, is the minor antibody derivative with a molecular weight of 15 kDa. The small size, excellent target recognition, and high affinity make sdAbs robust vectors for cancer imaging and treatment (10). We are devoted to engineering sdAb-based radiopharmaceuticals for routine clinical use and have successfully developed a series of novel diagnostic sdAb tracers (11,12). Clinical use of these tracers enables precise detection of metastatic cancers and will hopefully yield effective treatment outcomes.

The cluster of differentiation 70 (CD70), a member of the tumor necrosis factor superfamily 7, is a type II transmembrane surface antigen. It is only highly expressed in a small subgroup of activated memory T and B cells in normal conditions (13). Recent studies elucidated that CD70 is highly expressed in various solid tumors, especially in RCCs (14). Full-length therapeutic monoclonal antibodies and chimeric antigen receptor T-cell immunotherapies targeting CD70 have become research hotspots in treating RCC (15,16). A more recent clinical trial reported that allogeneic CD70 chimeric antigen receptor T-cells (i.e., CTX130) had a disease control rate of 81.3% in 16 patients with relapsed or refractory ccRCC (17). In this setting, the visual surveillance of CD70 expression could help diagnose ccRCC, administer

Received Jul. 29, 2024; revision accepted Oct. 2, 2024.
For correspondence or reprints, contact Weijun Wei (ww@shsmu.edu.cn) or Fang Xie (fangxie@fudan.edu.cn).
*Contributed equally to this work.
Published online Nov. 7, 2024.
COPYRIGHT © 2024 by the Society of Nuclear Medicine and Molecular Imaging.

CD70-targeted therapeutics, and monitor therapeutic responses after the treatments. We recently reported the first-generation CD70-targeting ^{18}F -based sdAb tracer, [^{18}F]RCCB6 (18,19), which readily detected ccRCC metastases competently compared with ^{18}F -FDG PET/CT. Although delivery options are available, the ^{18}F -based tracer synthesis requires a dedicated cyclotron. Since $^{68}\text{Ga}/^{68}\text{Ga}$ generators approved by the Food and Drug Administration are commercially available for the convenient production of ^{68}Ga , developing a ^{68}Ga -labeled tracer could help spread and broaden the use of the CD70-targeted imaging strategy. Moreover, ^{68}Ga -labeling technology is fast and robust, and ^{68}Ga -labeled tracers are more likely to be used as companion diagnostics, guiding subsequent radiopharmaceutical therapy (20).

In the current study, we first systematically explore and elucidate the expression of CD70 in different types of RCCs and the prognostic value in ccRCC. We then report the de novo synthesis, preclinical biologic evaluation, and clinical translation of ^{68}Ga -labeled CD70-specific sdAb imaging tracers.

MATERIALS AND METHODS

The online supplemental material describes all the materials and methods (supplemental materials are available at <http://jnm.snmjournals.org>) (21–24).

RESULTS

Expression Patterns and Clinicopathological Value of CD70 in RCC

Normal kidney tissues did not express CD70 (14), which is consistent with our immunohistochemical staining results using 20 normal kidney tissues. We performed immunohistochemical staining of 424 tumor specimens from RCC patients and found that 82.82% of ccRCCs expressed CD70, of which 52.28% were highly expressed. In comparison, only 37.29% of papillary RCC (pRCC) and 18.67% of chromophobe RCC (chRCC) expressed CD70 (Fig. 1A). CD70 expression was significantly higher in ccRCC (79.28 ± 87.09) than in pRCC (13.32 ± 33.83 , $P < 0.001$) and chRCC (5.214 ± 12.40 , $P < 0.001$) according to the H score (Fig. 1A). In ccRCC, the positive rate of CD70 expression was high in tumors with various differentiation grades as well as in metastatic lesions ($P = 0.097$; Fig. 1B; Supplemental Table 1), indicating that CD70 is a constantly expressed biomarker for ccRCC irrespective of the differentiation and metastasis status. The typical images of CD70 expression in normal kidneys and different pathologic types of RCC are shown in Supplemental Figure 1. CD70 expression was significantly correlated with sex, tumor thrombus, tumor differentiation, tumor necrosis, distant metastasis, and overall survival (Table 1). Survival analysis in 176 patients from our institution ($P = 0.0127$) and 878 patients

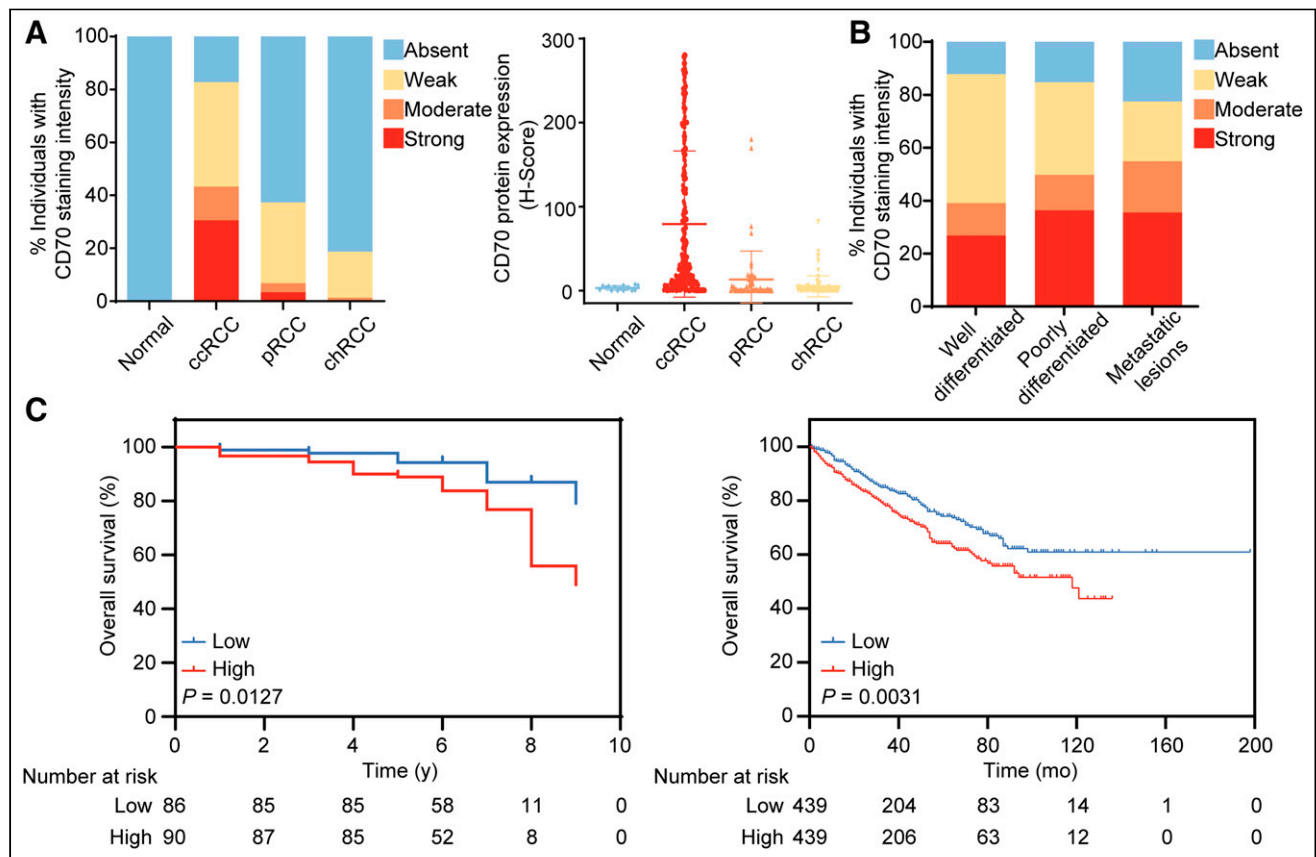


FIGURE 1. Immunohistochemical analysis of CD70 expression in RCC. (A) Percentage of different expression intensities of CD70 (left) and expression levels of CD70 according to H score (right) in different pathologic types of RCC and normal kidneys according to immunohistochemical staining intensity. (B) Percentage of varying expression intensities of CD70 in ccRCC with various differentiation and metastasis status. (C) Kaplan-Meier analysis of overall survival in 176 patients from our institution (left) and 878 patients from Cancer Genome Atlas (right) with RCC stratified by CD70 expression level.

TABLE 1
Relationship Between CD70 Expression and Clinicopathologic Characteristics in RCC

Variable	n	CD70 expression		P
		Low	High	
Age (y)				
<55	170	125	45	0.126
≥55	254	169	85	
Sex				
Female	132	105	27	0.002
Male	292	189	103	
Tumor size (cm)				
≤4	208	152	56	0.101
>4	216	142	74	
Lymph node metastasis				
Negative	342	244	98	0.067
Positive	82	50	32	
Tumor thrombus				
Negative	380	270	110	0.025
Positive	44	24	20	
Distant metastasis				
Negative	375	267	108	0.022
Positive	49	27	22	
Tumor differentiation				
Well-differentiated	243	205	38	<0.001
Poorly differentiated	181	109	72	
Tumor necrosis				
Absence	347	252	95	0.002
Presence	77	42	35	
Overall survival				
Survive	228	176	52	0.015
Death	51	31	20	

from the Cancer Genome Atlas with RCC ($P = 0.0031$) showed reduced overall survival in patients with high CD70 expression (Fig. 1C).

Synthesis and Characterization of [⁶⁸Ga]Ga-NOTA-RCCB3 and [⁶⁸Ga]Ga-NOTA-RCCB6

We previously reported 2 CD70-specific sdAbs (RCCB3 and RCCB6) in developing ¹⁸F-labeled tracers (18,19). We adapted these 2 clones to develop ⁶⁸Ga-labeled tracers in the study. Sodium dodecyl sulfate–polyacrylamide gel electrophoresis and high-performance liquid chromatography cross-validated the purity of these 2 sdAbs as greater than 90% with a molecular weight of 15 kDa (Figs. 2A and 2B). The binding ability of both clones to the recombinant human CD70 protein was evaluated using surface plasmon resonance assays (Figs. 2A and 2B; Supplemental Table 2). RCCB3 and RCCB6 exhibited strong binding affinity, a high binding rate constant, and a low dissociation rate constant with human CD70, with corresponding dissociation rates of 5.668 and 3.372 nM, respectively.

Preclinical [⁶⁸Ga]Ga-NOTA-RCCB3 and [⁶⁸Ga]Ga-NOTA-RCCB6 Immuno-PET/CT Imaging

The radiochemical purity of [⁶⁸Ga]Ga-NOTA-RCCB3 and [⁶⁸Ga]Ga-NOTA-RCCB6 was more than 99% (Supplemental Fig. 2). The non-decay-corrected radiolabeling yields of [⁶⁸Ga]Ga-NOTA-RCCB3 and [⁶⁸Ga]Ga-NOTA-RCCB6 were 34.8% and 46.8%, respectively, and the specific activities were 1,634.7 and 2,422.0 MBq/μmol, respectively. To investigate the diagnostic value of the 2 tracers, we established 2 ccRCC patient-derived xenograft (PDX) models (no. 62 PDX and no. 371 PDX). Immunohistochemical analysis verified the high expression of CD70 in these 2 models (Supplemental Fig. 3).

We first assessed the diagnostic power of [⁶⁸Ga]Ga-NOTA-RCCB3 and [⁶⁸Ga]Ga-NOTA-RCCB6 immuno-PET/CT in the subcutaneous no. 62 PDX model. Both tracers could visualize tumors 1 h after injection (Figs. 3A and 3B). For [⁶⁸Ga]Ga-NOTA-RCCB3 immuno-PET/CT imaging, analysis of the region-of-interest data showed an average tumor uptake of 3.57 ± 0.93 percentage of injected dose per gram (%ID/g) ($n = 3$). Kidney

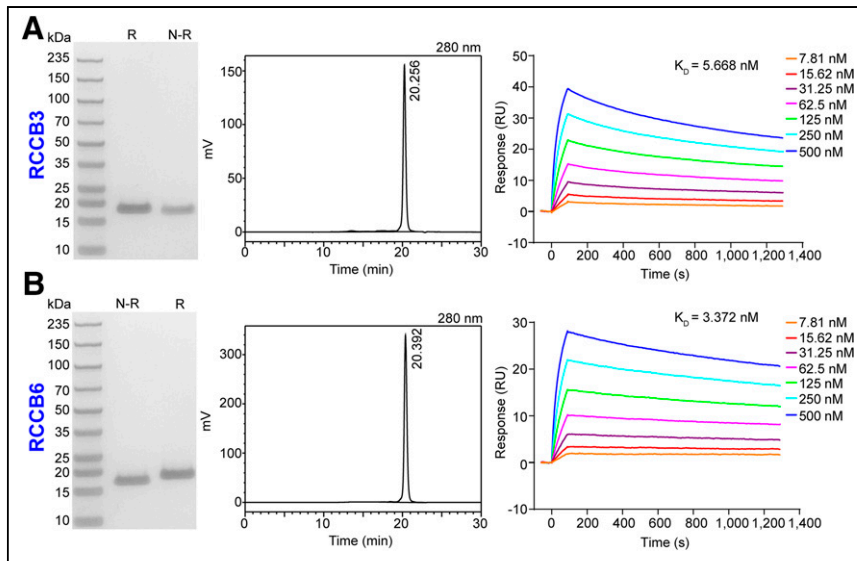


FIGURE 2. Expression and characterization of RCCB3 and RCCB6. (A) Sodium dodecyl sulfate–polyacrylamide gel electrophoresis (left), high-performance liquid chromatography (middle), and surface plasmon resonance (right) analysis results show purity and interacting curves of RCCB3 with recombinant human CD70 protein. (B) Sodium dodecyl sulfate–polyacrylamide gel electrophoresis (left), high-performance liquid chromatography (middle), and surface plasmon resonance (right) analysis results show purity and interacting curves of RCCB6 with recombinant human CD70 protein. K_D = dissociation constant; N-R = nonreducing condition; R = reducing condition; RU = response unit.

accumulation with an average value of 62.07 ± 25.42 %ID/g was high because of the rapid renal clearance, reabsorption, and retention of the tracer (Fig. 3A). The tumor-to-liver, tumor-to-kidney, tumor-to-blood, and tumor-to-muscle ratios were 1.11 ± 0.15 , 0.06 ± 0.01 , 1.75 ± 0.25 , and 4.97 ± 0.61 , respectively. Subsequent biodistribution confirmed the highest kidney accumulation of the tracer (167.01 ± 67.98 %ID/g), followed by the uptake in the tumor (3.29 ± 0.46 %ID/g) and liver (2.71 ± 0.96 %ID/g). Retention of the tracer in other normal tissues and organs was generally low. Similar imaging results were achieved using [^{68}Ga]Ga-NOTA-RCCB6 (Fig. 3B). Tumor uptake of [^{68}Ga]Ga-NOTA-RCCB6 on region-of-interest analysis (3.60 ± 0.70 %ID/g) was comparable to that of [^{68}Ga]Ga-NOTA-RCCB3 ($P = 0.97$).

Validation of [^{68}Ga]Ga-NOTA-RCCB6 Immuno-PET/CT Imaging Specificity

To determine the targeting specificity of [^{68}Ga]Ga-NOTA-RCCB6 toward CD70, we did a blocking study in another group of tumor-bearing mice. Mice in the blocking group were administered ABDB6 (Supplemental Fig. 4), an RCCB6 derivative capable of simultaneously binding to serum albumin and human CD70, to saturate CD70 molecules on tumor cells. [^{68}Ga]Ga-NOTA-RCCB6 immuno-PET/CT imaging performed 2 d after ABDB6 blockade showed an average tumor uptake of 0.93 ± 0.34 %ID/g ($n = 3$), which was significantly lower than that in the nonblocking group ($P = 0.008$; Fig. 3C). We further performed immuno-PET/CT imaging with [^{68}Ga]Ga-NOTA-RCCB6 and [^{68}Ga]Ga-NOTA-R5C (a negative tracer derived from a nonspecific sdAb R5C; Supplemental Fig. 5) in the no. 371 PDX model with higher CD70 expression. Immuno-PET/CT imaging with [^{68}Ga]Ga-NOTA-RCCB6 (Fig. 4A), but not with [^{68}Ga]Ga-NOTA-R5C (Fig. 4B), clearly delineated a subcutaneously inoculated tumor. Region-of-interest analysis further revealed prominent tumor uptake of [^{68}Ga]Ga-NOTA-RCCB6

(19.53 ± 1.86 %ID/g, $n = 3$; Fig. 4A) compared with uptake of [^{68}Ga]Ga-NOTA-R5C (1.34 ± 0.85 %ID/g, $n = 3$; Fig. 4B) in the no. 371 ccRCC PDX model. Thus, the specificity of [^{68}Ga]Ga-NOTA-RCCB6 in targeting CD70 was cross-validated.

Immunohistochemical staining was performed to determine the expression of CD70 after the imaging studies. Higher membranous CD70 expression was found in the no. 371 model than in the no. 62 PDX model (Supplemental Fig. 6), consistent with the above imaging findings. Both [^{68}Ga]Ga-NOTA-RCCB3 and [^{68}Ga]Ga-NOTA-RCCB6 exhibited good diagnostic value in preclinical ccRCC models, with the specificity of [^{68}Ga]Ga-NOTA-RCCB6 thoroughly validated.

Distribution of [^{68}Ga]Ga-NOTA-RCCB6 and [^{68}Ga]Ga-NOTA-RCCB3 in RCC Patients

In a prospective clinical trial approved by the institutional review board of the Huashan Hospital, Fudan University, and registered at ClinicalTrials.gov (NCT06148220), we investigated the feasibility, safety, and preliminary diagnostic value of [^{68}Ga]Ga-NOTA-RCCB6 and [^{68}Ga]Ga-NOTA-RCCB3 immuno-PET/CT imaging, especially the former tracer. The institutional review board approved this study, and all subjects provided written informed consent. Eight men (age range, 51–71 y) were recruited, all with pathologically confirmed RCC (Supplemental Table 3). Seven of these patients underwent [^{68}Ga]Ga-NOTA-RCCB6 immuno-PET/CT imaging, whereas another received [^{68}Ga]Ga-NOTA-RCCB3 imaging. None of the patients experienced significant acute or chronic toxic reactions during the study period. Of 4 patients having tissues for CD70 staining, 3 patients were CD70-positive (patients 1, 2, and 8), whereas patient 4 was negative. Overall, [^{68}Ga]Ga-NOTA-RCCB6 was rapidly cleared from the urinary system, with high uptake found in the kidneys and bladder with an SUV_{max} of 129.94 ± 18.57 and 26.60 ± 23.03 , respectively. Minor uptake was found in the spleen and heart with an SUV_{max} of 2.79 ± 1.24 and 1.89 ± 0.22 , respectively. Low uptake was found in the salivary glands, thyroid, brain, intestine, and liver with the corresponding SUV_{max} of 1.24 ± 0.24 , 1.03 ± 0.26 , 0.27 ± 0.43 , 1.73 ± 0.86 , and 1.73 ± 0.86 , respectively (Supplemental Fig. 7). The low background signal of the 2 tracers lays a solid foundation for detecting ccRCC metastases.

Preliminary Diagnostic Value of [^{68}Ga]Ga-NOTA-RCCB3 and [^{68}Ga]Ga-NOTA-RCCB6

Patient 2 was a 71-y-old man who underwent radical surgery for right renal carcinoma in 2016 with the pathologic finding of grade 2 to 3 ccRCC, underwent resection of a right adrenal metastases in 2019, and then developed multiple thyroid and liver metastases in 2021. The patient received sequential ^{18}F -FDG PET/CT and [^{68}Ga]Ga-NOTA-RCCB6 immuno-PET/CT imaging for comprehensive evaluation (Fig. 5A). [^{68}Ga]Ga-NOTA-RCCB6 immuno-PET/CT revealed additional metastatic lesions in the right erector spinae (SUV_{max} , 7.1) and right gluteus maximus (SUV_{max} , 6.62), which were not visualized on ^{18}F -FDG PET/CT or conventional CT/MRI. [^{68}Ga]Ga-NOTA-RCCB6 uptake in metastases

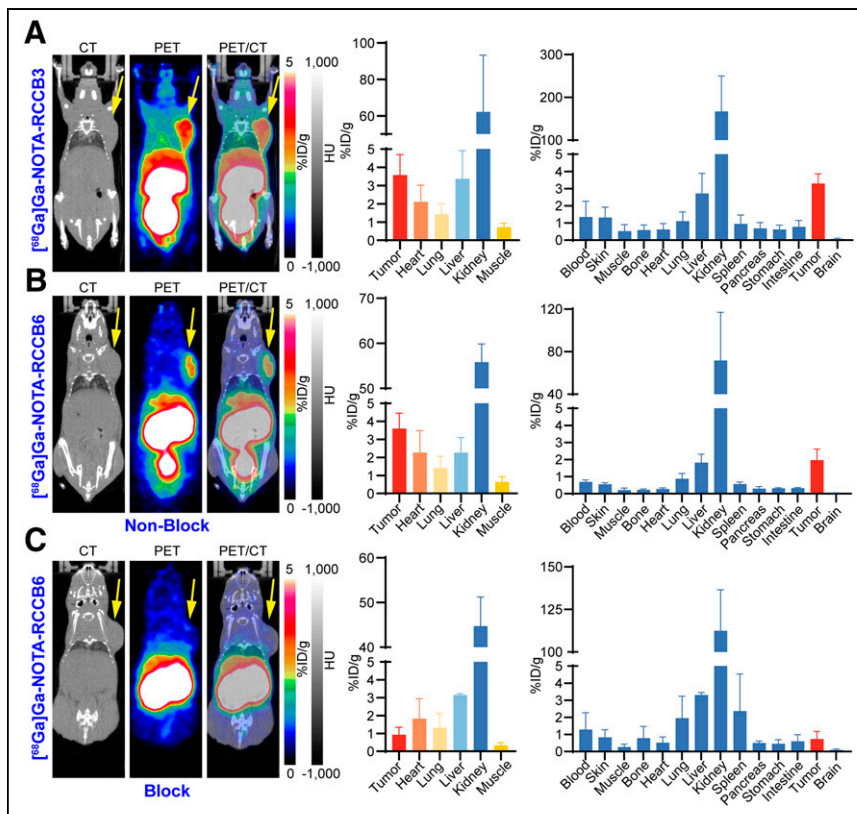


FIGURE 3. $[^{68}\text{Ga}]\text{Ga-NOTA-RCCB3}$ and $[^{68}\text{Ga}]\text{Ga-NOTA-RCCB6}$ immuno-PET/CT imaging in subcutaneous no. 62 PDX ccRCC model. (A) $[^{68}\text{Ga}]\text{Ga-NOTA-RCCB3}$ immuno-PET/CT images (left) in subcutaneous ccRCC model 1 h after injection. Region-of-interest data (middle) and radioactive biodistribution results (right) of $[^{68}\text{Ga}]\text{Ga-NOTA-RCCB3}$ in tumors and major organs of ccRCC model. (B) $[^{68}\text{Ga}]\text{Ga-NOTA-RCCB6}$ immuno-PET/CT images (left) in subcutaneous ccRCC model 1 h after injection. Region-of-interest data (middle) and radioactive biodistribution results (right) of $[^{68}\text{Ga}]\text{Ga-NOTA-RCCB6}$ in tumors and major organs of ccRCC model. (C) $[^{68}\text{Ga}]\text{Ga-NOTA-RCCB6}$ immuno-PET/CT images (left) in ABDB6 blocking group. Region-of-interest data (middle) and radioactive biodistribution results (right) of $[^{68}\text{Ga}]\text{Ga-NOTA-RCCB6}$ in tumors and major organs of ccRCC model. Tumors were displayed on coronal images, indicated by arrows. HU = Hounsfield unit.

was generally higher than that of $^{18}\text{F-FDG}$: thyroid metastases (6.24 vs. 3.82), liver metastases (15.76 \pm 8.53 vs. 3.06 \pm 0.51), and pancreatic metastases (20.81 vs. 5.66). Hematoxylin and eosin staining and immunohistochemical staining of the patient's primary tumor and right adrenal metastasis confirmed ccRCC pathology and positive staining of CD70 (Fig. 5B; Supplemental Fig. 8).

Patient 4 was a 68-y-old man undergoing left renal tumor resection with the pathology of type 2 grade 2 pRCC in 2018; the patient then suffered from recurrence on the left posterior renal hiatus and left pararenal, retroperitoneal lymph node metastases, and left upper-lobe metastases since 2022, which were evident on $^{18}\text{F-FDG}$ PET/CT (Supplemental Fig. 9). There was no $[^{68}\text{Ga}]\text{Ga-NOTA-RCCB6}$ uptake in the recurrence and metastases of the patient (Fig. 6A). The SUV_{max} of $[^{68}\text{Ga}]\text{Ga-NOTA-RCCB6}$ in the left lung and the parbasal abdominal aortic lymph node lesions was 0.95 and 1.13, respectively. Hematoxylin and eosin staining and immunohistochemical staining of the patient's primary tumor validated pRCC and negative staining of CD70 (Fig. 6B).

Patient 7 was a 66-y-old man with a left renal mass detected in 2021. Biopsy pathology confirmed ccRCC, and the patient received targeted therapy and immunotherapy since then. The patient underwent $[^{68}\text{Ga}]\text{Ga-NOTA-RCCB6}$ immuno-PET/CT imaging to evaluate

the treatment efficacy, which demonstrated that the left renal tumor did not have tracer uptake with an SUV_{max} of 1.76 (Supplemental Figs. 10A and 10B). The patient underwent a left nephrectomy 2 mo later, and the pathology suggested no residual tumor (Supplemental Fig. 10C). Patient 8 was a 60-y-old man who underwent renal tumor resection in 2014 and left lung metastasis resection in 2023 with a pathology of grade 2 to 3 ccRCC. He received $[^{68}\text{Ga}]\text{Ga-NOTA-RCCB3}$ immuno-PET/CT imaging for routine postsurgery surveillance, which revealed unexpected multiple microlung nodules with uptake (Supplemental Figs. 11A and 11B). Since immunohistochemical staining of the patient's primary tumor showed positive staining of CD70, these newly identified microlung nodules with $[^{68}\text{Ga}]\text{Ga-NOTA-RCCB3}$ uptake were deemed metastases (Supplemental Fig. 11C).

DISCUSSION

CD70 is a transmembrane protein generally expressed on the surface of activated T and B cells in response to antigenic stimulation without sustained expression. A study by Ruf et al. found that 78% of ccRCC and 32% of pRCC expressed CD70, whereas normal kidneys had no expression (25). Our retrospective study confirmed that CD70 was not expressed in normal kidneys, and the positive rate of CD70 was up to 82.82% in ccRCC with a higher H score ($P < 0.001$) but was low in pRCC and chRCC. Moreover, CD70-positive rates were high in well-differentiated (87.5%), poorly differentiated (85.19%), and metastatic (77.42%) ccRCCs. Furthermore, the expression level of CD70 is unaffected by tumor differentiation or metastasis status. A retrospective analysis further showed that CD70 expression was strongly correlated with sex, tumor differentiation, tumor thrombus, necrosis, distant metastasis, and overall survival in RCC. Other studies confirmed that CD70 is an oncogene that promotes tumor invasion and metastasis and is associated with poor patient prognosis (25,26). From the available evidence, we can conclude that CD70 is a promising theranostic target for RCC, especially for ccRCC. Indeed, diagnostics and therapeutics targeting CD70 are under clinical investigation (17,18).

In this study, we synthesized 2 novel sdAb tracers, $[^{68}\text{Ga}]\text{Ga-NOTA-RCCB3}$ and $[^{68}\text{Ga}]\text{Ga-NOTA-RCCB6}$, and evaluated the diagnostic potential in the preclinical no. 62 ccRCC PDX model. The average tumor uptake of the 2 tracers was 3.57 ± 0.93 and 3.60 ± 0.70 %ID/g 1 h after injection. The targeting potency and specificity of $[^{68}\text{Ga}]\text{Ga-NOTA-RCCB6}$ were further validated by an ABDB6 blocking study and comparative imaging study in the no. 371 ccRCC PDX model. On the basis of preclinical data, we designed a first-in-human study evaluating the clinical feasibility and diagnostic value of the developed CD70-targeted imaging approaches. $[^{68}\text{Ga}]\text{Ga-NOTA-RCCB6}$ immuno-PET/CT imaging

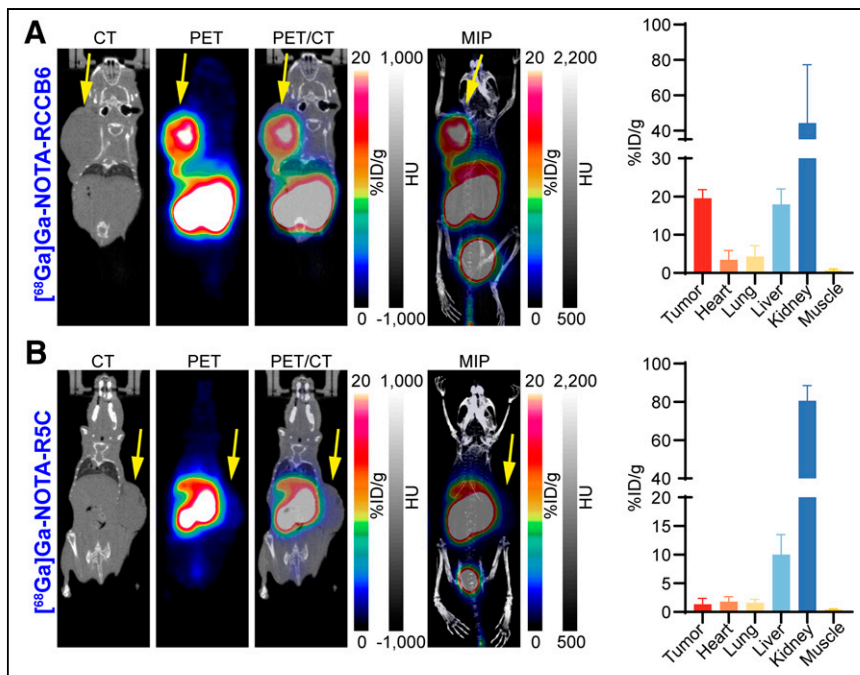


FIGURE 4. $[^{68}\text{Ga}]\text{Ga-NOTA-RCCB6}$ and $[^{68}\text{Ga}]\text{Ga-NOTA-R5C}$ immuno-PET/CT imaging in subcutaneous no. 371 PDX ccRCC model. (A) $[^{68}\text{Ga}]\text{Ga-NOTA-RCCB6}$ immuno-PET/CT images (left) in subcutaneous ccRCC model 1 h after injection. Region-of-interest data (right) of $[^{68}\text{Ga}]\text{Ga-NOTA-RCCB6}$ in tumors and major organs of ccRCC model. (B) $[^{68}\text{Ga}]\text{Ga-NOTA-R5C}$ immuno-PET/CT images (left) in subcutaneous ccRCC model 1 h after injection. Region-of-interest data (right) of $[^{68}\text{Ga}]\text{Ga-NOTA-R5C}$ in tumors and major organs of ccRCC model. Tumors were displayed on coronal images, indicated by arrows. HU = Hounsfield unit.

was performed in 7 RCC patients with suspected metastases. Uptake of $[^{68}\text{Ga}]\text{Ga-NOTA-RCCB6}$ was significantly higher in CD70-positive lesions ($\text{SUV}_{\text{max}}, 10.62 \pm 7.77$) than in CD70-negative lesions ($\text{SUV}_{\text{max}}, 1.04 \pm 0.09, P < 0.05$). Preliminary data suggested that $[^{68}\text{Ga}]\text{Ga-NOTA-RCCB6}$ immuno-PET/CT imaging could demonstrate the number and location of ccRCC metastases, including those not evident on conventional imaging examinations. The novel imaging approach may also be used in postoperative follow-up to monitor recurrence and metastasis. As companion diagnostics, $[^{68}\text{Ga}]\text{Ga-NOTA-RCCB6}$ immuno-PET/CT may be used for whole-body CD70 visualization, CD70-specific patient selection, and response monitoring. Our tissue microarray staining results indicated low expression abundance and proportion of CD70 in pRCC. In a pRCC patient with lung and retroperitoneal metastases, $[^{68}\text{Ga}]\text{Ga-NOTA-RCCB6}$ showed negative uptake in metastatic lesions, whereas $^{18}\text{F-FDG}$ had positive uptake, indicating the limited value of the CD70-targeted tracer in detecting pRCC metastases. The correlation between $[^{68}\text{Ga}]\text{Ga-NOTA-RCCB6}$ uptake and the CD70 expression level could not be calculated with the small sample size. We are actively recruiting

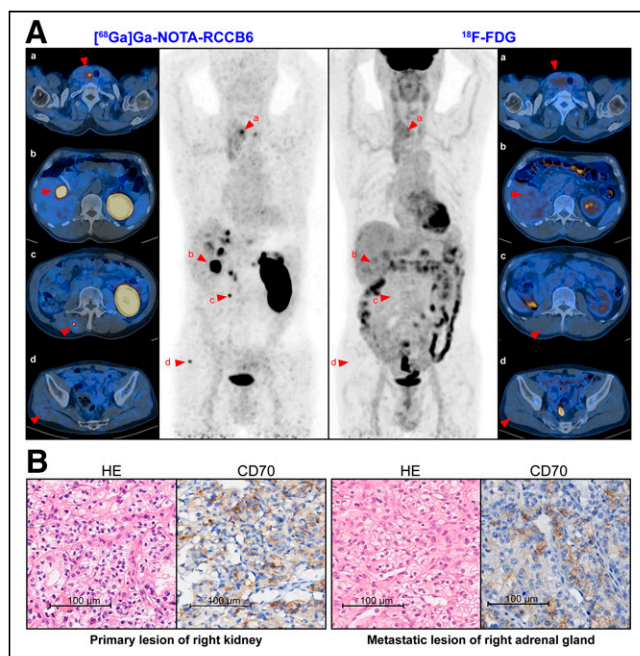


FIGURE 5. $[^{68}\text{Ga}]\text{Ga-NOTA-RCCB6}$ and $^{18}\text{F-FDG}$ PET/CT images in CD70-positive RCC patient. (A) Maximum-intensity projection and fused PET/CT images of $[^{68}\text{Ga}]\text{Ga-NOTA-RCCB6}$ (left) and $^{18}\text{F-FDG}$ (right) in patient 2. Metastases in thyroid, liver, right erector spinae, and right gluteus maximus (arrowheads) were displayed by $[^{68}\text{Ga}]\text{Ga-NOTA-RCCB6}$ but not by $^{18}\text{F-FDG}$. (B) Hematoxylin and eosin (HE) staining and CD70 immunohistochemical staining of patient's primary lesion and right adrenal metastatic lesion.

patients to participate in our ongoing clinical trial and will be able to draw the correlation in future studies.

As a tumor-specific marker that was hotly investigated, CD70 was confirmed to be aberrantly expressed in various tumors (27). Previous studies have shown that CD70 on tumor cells could bind to its receptor CD27 on lymphocytes, resulting in immunosuppression by inducing apoptosis of immune effector cells in the tumor microenvironment (28). The high expression of CD70 in ccRCC, a kind of immuno-hot tumor, might be associated with its immune microenvironment, which warrants further investigation. Targeting CD70 to eliminate CD70-positive tumor cells or to block the CD70–CD27 signaling axis was a possible direction for ccRCC treatment. Full-length monoclonal antibodies, antibody–drug conjugates targeting CD70, and anti-CD70 chimeric antigen receptor T-cell therapies in patients with advanced ccRCC have entered clinical trials (29–31). $[^{68}\text{Ga}]\text{Ga-NOTA-RCCB6}$ immuno-PET imaging allowed noninvasive visualization of CD70 expression, which could help in selecting ccRCC patients for whom CD70-targeted therapies may be suitable and evaluating the efficacy of these therapies.

A common feature of low-molecular-weight molecular imaging tracers is the high kidney accumulation (10). SdAb is the most minor antibody derivative and is well-suited for same-day molecular imaging. Rapid clearance, glomerular filtration, and renal reabsorption lead to a high accumulation of sdAb tracers and impaired efficacy in diagnosing primary urinary tumors, including RCCs. High accumulation of $[^{68}\text{Ga}]\text{Ga-NOTA-RCCB6}$ in the kidneys hinders the detection of primary RCC. Strategies such as albumin binder incorporation and PEGylation have been exploited to improve the pharmacokinetics and pharmacodynamics of sdAb radiopharmaceuticals (32,33). In the efforts to develop therapeutic

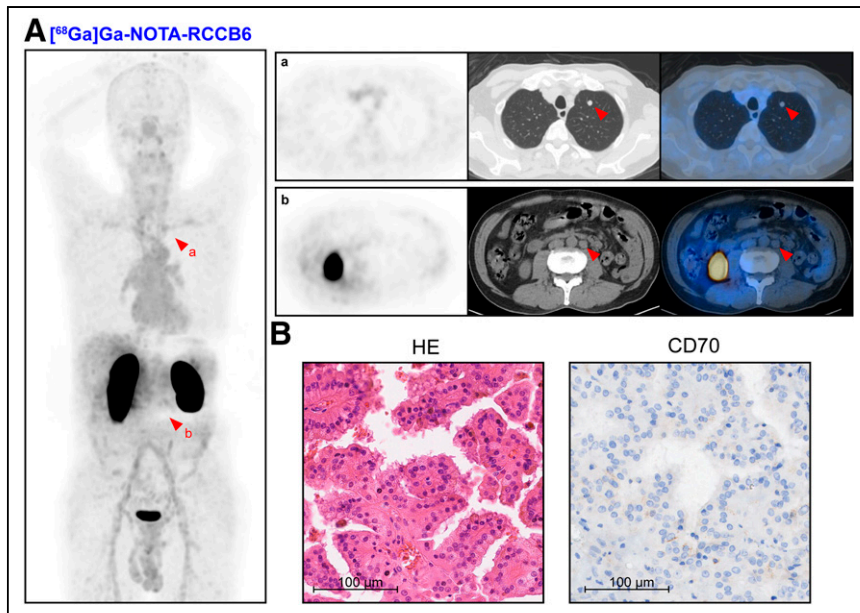


FIGURE 6. [^{68}Ga]Ga-NOTA-RCCB6 immuno-PET/CT imaging in CD70-negative pRCC patient. (A) Maximum-intensity projection image (left) and PET/CT images (right) of [^{68}Ga]Ga-NOTA-RCCB6 in patient 4 show metastatic lesions (arrowheads) with no uptake in upper lobe of left lung and retroperitoneal lymph node. (B) Hematoxylin and eosin (HE) staining and CD70 immunohistochemical staining of primary lesion of patient show negative CD70 staining.

radiopharmaceuticals targeting CD70, we have successfully engineered ABDB6 with an extended in vivo half-life and full retention of biologic activity. ABDB6-derived radiopharmaceuticals will facilitate the detection of primary ccRCC from the diagnostic perspective and have an improved therapeutic index from a treatment perspective. Several radionuclides, such as ^{177}Lu , ^{225}Ac , and ^{211}At , are being used to develop CD70-targeted radiopharmaceutical therapy agents.

CONCLUSION

This work developed and characterized 2 novel CD70-specific sdAb tracers ([^{68}Ga]Ga-NOTA-RCCB3 and [^{68}Ga]Ga-NOTA-RCCB6). Preliminary clinical trial results demonstrated the value of [^{68}Ga]Ga-NOTA-RCCB6 immuno-PET/CT imaging in monitoring ccRCC metastasis and recurrence in postsurgery settings.

KEY POINTS

QUESTION: What are the expression characteristics of CD70 in RCCs, and does CD70-targeted immuno-PET/CT have diagnostic value in RCCs?

PERTINENT FINDINGS: After analyzing 424 RCC specimens, we found that CD70 is highly and constantly expressed in ccRCC and is associated with poor patient survival. Immuno-PET/CT imaging with [^{68}Ga]Ga-NOTA-RCCB3 or [^{68}Ga]Ga-NOTA-RCCB6 has definite value in visualizing CD70 expression and differentiating ccRCC from other RCCs.

IMPLICATIONS FOR PATIENT CARE: By noninvasively annotating CD70 expression, [^{68}Ga]Ga-NOTA-RCCB6 and [^{68}Ga]Ga-NOTA-RCCB3 immuno-PET/CT imaging will optimize the management of ccRCC by facilitating target-specific diagnosis of ccRCC metastases, selecting patients suitable for CD70-targeted therapies, and monitoring responses after the treatments.

DISCLOSURE

The work was partly supported by the National Key Research and Development Program of China (Grant no. 2020YFA0909000) and the National Natural Science Foundation of China (Grant Nos. 82372014 and 82402322).

REFERENCES

- Sung H, Ferlay J, Siegel RL, et al. Global cancer statistics 2020: GLOBOCAN estimates of incidence and mortality worldwide for 36 cancers in 185 countries. *CA Cancer J Clin.* 2021;71:209–249.
- Singh D. Current updates and future perspectives on the management of renal cell carcinoma. *Life Sci.* 2021;264:118632.
- Bukavina L, Bensalah K, Bray F, et al. Epidemiology of renal cell carcinoma: 2022 update. *Eur Urol.* 2022;82:529–542.
- Dabestani S, Thorstenson A, Lindblad P, Harmenberg U, Ljungberg B, Lundstam S. Renal cell carcinoma recurrences and metastases in primary non-metastatic patients: a population-based study. *World J Urol.* 2016;34:1081–1086.
- Iravani A, Hicks RJ. Imaging the cancer immune environment and its response to pharmacologic intervention, part 1: the role of ^{18}F -FDG PET/CT. *J Nucl Med.* 2020;61:943–950.
- Escudier B, Porta C, Schmidinger M, et al. Renal cell carcinoma: ESMO clinical practice guidelines for diagnosis, treatment and follow-up. *Ann Oncol.* 2019;30:706–720.
- Roussel E, Capitanio U, Kutikov A, et al. Novel imaging methods for renal mass characterization: a collaborative review. *Eur Urol.* 2022;81:476–488.
- Shuch B, Pantuck AJ, Bernhard JC, et al. [^{89}Zr]Zr-girentuximab for PET-CT imaging of clear-cell renal cell carcinoma: a prospective, open-label, multicentre, phase 3 trial. *Lancet Oncol.* 2024;25:1277–1287.
- Verhoeff SR, van Es SC, Boon E, et al. Lesion detection by [^{89}Zr]Zr-DFO-girentuximab and [^{18}F]FDG-PET/CT in patients with newly diagnosed metastatic renal cell carcinoma. *Eur J Nucl Med Mol Imaging.* 2019;46:1931–1939.
- Wei W, Younis MH, Lan X, Liu J, Cai W. Single-domain antibody theranostics on the horizon. *J Nucl Med.* 2022;63:1475–1479.
- Huang W, Zhang Y, Cao M, et al. ImmunoPET imaging of Trop2 in patients with solid tumours. *EMBO Mol Med.* 2024;16:1143–1161.
- Zhang Y, Cao M, Wu Y, et al. Preclinical development of novel PD-L1 tracers and first-in-human study of [^{68}Ga]Ga-NOTA-RW102 in patients with lung cancers. *J Immunother Cancer.* 2024;12:e008794.
- Flieswasser T, Van den Eynde A, Van Audenaerde J, et al. The CD70-CD27 axis in oncology: the new kids on the block. *J Exp Clin Cancer Res.* 2022;41:12.
- Jilaveanu LB, Sznol J, Aziz SA, Duchon D, Kluger HM, Camp RL. CD70 expression patterns in renal cell carcinoma. *Hum Pathol.* 2012;43:1394–1399.
- Silence K, Dreier T, Moshir M, et al. ARGX-110, a highly potent antibody targeting CD70, eliminates tumors via both enhanced ADCC and immune checkpoint blockade. *MAbs.* 2014;6:523–532.
- Panowski SH, Srinivasan S, Tan N, et al. Preclinical development and evaluation of allogeneic CAR T cells targeting CD70 for the treatment of renal cell carcinoma. *Cancer Res.* 2022;82:2610–2624.
- Pal SK, Tran B, Haanen J, et al. CD70-targeted allogeneic CAR T-cell therapy for advanced clear cell renal cell carcinoma. *Cancer Discov.* 2024;14:1176–1189.
- Wu Q, Wu Y, Zhang Y, et al. ImmunoPET/CT imaging of clear cell renal cell carcinoma with [^{18}F]RCCB6: a first-in-human study. *Eur J Nucl Med Mol Imaging.* 2024;51:2444–2457.
- Wu Q, Wu Y, Zhang Y, et al. [^{18}F]RCCB6 immuno-positron emission tomography/computed tomography for postoperative surveillance in clear cell renal cell carcinoma: a pilot clinical study. *Eur Urol.* 2024;86:372–374.
- Akhavanlalf A, Peterson AB, Fitzpatrick K, et al. The predictive value of pretherapy [^{68}Ga]Ga-DOTA-TATE PET and biomarkers in [^{177}Lu]Lu-PRRT tumor dosimetry. *Eur J Nucl Med Mol Imaging.* 2023;50:2984–2996.

21. Tang Z, Li C, Kang B, Gao G, Li C, Zhang Z. GEPIA: a web server for cancer and normal gene expression profiling and interactive analyses. *Nucleic Acids Res.* 2017;45:W98–W102.
22. Garousi J, von Witting E, Borin J, et al. Radionuclide therapy using ABD-fused ADAPT scaffold protein: proof of principle. *Biomaterials.* 2021;266:120381.
23. An S, Zhang D, Zhang Y, et al. GPC3-targeted immunoPET imaging of hepatocellular carcinomas. *Eur J Nucl Med Mol Imaging.* 2022;49:2682–2692.
24. Specht E, Kaemmerer D, Sanger J, Wirtz RM, Schulz S, Lupp A. Comparison of immunoreactive score, HER2/neu score and H score for the immunohistochemical evaluation of somatostatin receptors in bronchopulmonary neuroendocrine neoplasms. *Histopathology.* 2015;67:368–377.
25. Ruf M, Mittmann C, Nowicka AM, et al. pVHL/HIF-regulated CD70 expression is associated with infiltration of CD27+ lymphocytes and increased serum levels of soluble CD27 in clear cell renal cell carcinoma. *Clin Cancer Res.* 2015;21:889–898.
26. Alchahin AM, Mei S, Tsea I, et al. A transcriptional metastatic signature predicts survival in clear cell renal cell carcinoma. *Nat Commun.* 2022;13:5747.
27. Jacobs J, Deschoolmeester V, Zwaenepoel K, et al. CD70: an emerging target in cancer immunotherapy. *Pharmacol Ther.* 2015;155:1–10.
28. Yang ZZ, Grote DM, Xiu B, et al. TGF- β upregulates CD70 expression and induces exhaustion of effector memory T cells in B-cell non-Hodgkin's lymphoma. *Leukemia.* 2014;28:1872–1884.
29. Pal SK, Forero-Torres A, Thompson JA, et al. A phase I trial of SGN-CD70A in patients with CD70-positive, metastatic renal cell carcinoma. *Cancer.* 2019;125:1124–1132.
30. Ochsenbein AF, Riether C, Bacher U, et al. Argx-110 targeting CD70, in combination with azacitidine, shows favorable safety profile and promising anti-leukemia activity in newly diagnosed AML patients in an ongoing phase 1/2 clinical trial. *Blood.* 2018;132 (suppl 1):2680.
31. Yang M, Tang X, Zhang Z, et al. Tandem CAR-T cells targeting CD70 and B7-H3 exhibit potent preclinical activity against multiple solid tumors. *Theranostics.* 2020;10:7622–7634.
32. Zhang Y, Zhang D, An S, et al. Development and characterization of nanobody-derived CD47 theranostic pairs in solid tumors. *Research (Wash D C).* 2023;6:0077.
33. Rashidian M, Ingram JR, Dougan M, et al. Predicting the response to CTLA-4 blockade by longitudinal noninvasive monitoring of CD8 T cells. *J Exp Med.* 2017;214:2243–2255.